AIAA 2000-2418

ANALYSIS OF THE POWER BUDGET AND STABILITY OF HIGH-PRESSURE NONEQUILIBRIUM AIR PLASMAS

Igor V. Adamovich, J. William Rich,
Andrey P. Chernukho, and Serguei A. Zhdanok

Nonequilibrium Thermodynamics Laboratory
Dept. of Mechanical Engineering
The Ohio State University, Columbus, OH 43220-1107

Chemical Physics Laboratory, Department of Nonequilibrium Processes,
A.V. Lykov Heat and Mass Transfer Institute of Belarusian Academy of Sciences
Minsk, Belarus

31st AIAA Plasmadynamics and Lasers Conference
19 - 22 June 2000 / Denver, CO

AIAA 2000-2418

ANALYSIS OF THE POWER BUDGET AND STABILITY OF HIGH-PRESSURE NONEQUILIBRIUM AIR PLASMAS[1]

Igor V. Adamovich[2], J. William Rich[3],

Nonequilibrium Thermodynamics Laboratory, Dept. of Mechanical Engineering
The Ohio State University, Columbus, OH 43220-1107

Andrey P. Chernukho[4], and Serguei A. Zhdanok[5]

Chemical Physics Laboratory, Department of Nonequilibrium Processes,
A.V. Lykov Heat and Mass Transfer Institute of Belarusian Academy of Sciences
Minsk, Belarus

Abstract

The paper discusses the power budget and the stability of the high-pressure, high electron density, nonequilibrium air plasmas. Calculations using a detailed state-specific one-dimensional kinetic model show that, if ionization in the plasma is produced by an external electric field, an electron density of $n_e=10^{13}$ cm^{-3} is sustained at the power budget of more than 30 GW/m^3. This is due to the extremely low ionization efficiency (less than 0.1%) in nonequilibrium electric discharges. Therefore, the sole use of large-volume self-sustained discharges, whether the electric field is DC, RF, or microwave, is not feasible from the energy efficiency point of view. The plasma power budget can be substantially reduced by using an efficient external ionization source, such as an e-beam (ionization efficiency up to 40-50%). This will require 60 MW/m^3 to sustain electron density of $n_e=10^{13}$ cm^{-3}.

Calculations using a quasi-one-dimensional kinetic model suggest that the required electron density is reached under conditions where plasma collapse may be likely and glow-to-arc transition may be difficult to control over long distances. This occurs due to strong coupling between ionization and heating. However, analysis of the experiments in the high-voltage atmospheric pressure discharge in air, as well as calculations using a two-dimensional model of the discharge show that the use of the ballast resistor stabilization allows sustaining a stable constricted nonequilibrium atmospheric pressure air discharge well into the arc transition regime. The region occupied by the constricted discharge is a few cm long and a few mm in diameter. The diameter of the plasma is primarily controlled by the ambipolar diffusion of the charged species out of the high-current region. The results of calculations show that the two-dimensional kinetic model used gives an adequate description of the kinetics and the energy balance of the high-voltage atmospheric pressure discharge in air.

1. Introduction

Sustaining large-volume plasmas in atmospheric pressure air presents an extremely challenging problem. Among the most critical technical issues that have to be addressed to resolve this problem are the plasma power budget and stability. Numerous aerospace applications such as supersonic flow control, supersonic combustion control, and nonequilibrium MHD propulsion require an ability to initiate and

[2] Visiting Assistant Professor, Senior Member AIAA
[3] Ralph W. Kurtz Professor of Mechanical Engineering, Associate Fellow AIAA
[4] Senior Research Associate
[5] Department Head

sustain large volume (~1 m^3), relatively cold (T<2000 K) diffuse plasmas in atmospheric air, with electron density up to $n_e \sim 10^{13}$ cm^{-3}. For these applications, a power budget of the order of 1–10 MW/m^3 is desired. Finally, these plasma conditions are to be maintained for relatively long times, at least for 10 msec.

These goals define a highly nonequilibrium molecular plasma. The simultaneous requirement of electron densities of 10^{13} cm^{-3} and gas temperatures at 2,000 K represent an enormous departure from thermodynamic equilibrium, and rule out the use of purely thermal plasmas, such as high temperature arc discharges, to achieve this result. This can be illustrated by simple estimates using the Saha equation for a thermal equilibrium air plasma. For example, to achieve the stated electron density by merely heating the air, a gas temperature of ~ 4300 K would have to be maintained. Conversely, if atmospheric-pressure air were maintained at only the desired maximum gas temperature of 2000 K, the equilibrium electron density would be only ~ 10^6 cm^{-3}, many orders of magnitude below the desired value.

The preceding requirements have mandated examination of approaches using low-temperature nonequilibrium plasmas, of the general type characterized as glow discharges. Such systems have long been demonstrated to provide highly nonequilibrium plasmas, with relatively high free electron densities, with the requisite lower gas temperatures. However, if self-sustained discharges, lacking an external ionization source, are used, such glows are usually only struck at low pressures, well below even 0.1 atm pressure. Various methods have been used to extend the range of such self-sustained discharges to near atmospheric pressures, such as the use of individually ballasted multiple cathodes, short duration radio frequency high-voltage pulse stabilization, or aerodynamic stabilization [1-4]. Typically, however, the energy efficiency of such discharges is much lower than desired for the present goal, since only a small fraction of the input electrical power goes into ionization. As an example of operation of a nonequilibrium atmospheric pressure discharge in air, the present paper discusses earlier experimental results obtained at Chemical Physics Laboratory of A.V.Lykov Heat and Mass Transfer Institute in Minsk, Belarus [5-9]. The kinetics and energy balance in this strongly spatially nonuniform discharge are analyzed using a two-dimensional nonequilibrium flow code coupled with the key relaxation and chemical processes occurring in the air plasma, developed at Ohio State.

An alternative approach is the use of non-self-sustained glow discharges, in which some or all of the required volume ionization is provided by an external source, such as an electron beam [10,11]. Electron beams are identified as having by far the lowest power budget among all nonequilibrium ionization methods. Further, reliance on an external ionization source mitigates another principal difficulty known to exist in high-pressure discharges at large current densities. The well-known glow-to-arc-transition, with subsequent plasma thermalization, can be significantly delayed or avoided altogether. Finally, recent experiments in nonequilibrium plasmas optically pumped by a CO laser suggest a possibility of modification of electron removal rates in non-self-sustained plasmas by controlling metastable species concentrations and excited state populations [12,13]. This effect can be used to significantly reduce the power budget of electron beam sustained plasmas.

Quantitative prediction of the power budget of high-pressure air plasmas requires a model that contains not only realistic chemistry rates for the neutral and ionic species, but also processes of production and decay of excited metastable states, in particular vibrational states, and their coupling with free electrons. These latter features are essential for air plasmas, inasmuch as the free electron energies are closely coupled with the nitrogen and oxygen vibrational modes. Under these circumstances, it is impossible to transfer energy from an imposed electric discharge field to free electrons without also exciting molecular vibrational states. Accordingly, a rather detailed kinetic model of the air plasma is used for the quantitative analysis of the power budget.

2. Power budget of self-sustained and non-self-sustained air discharges

To evaluate the power budget of nonequilibrium atmospheric air plasmas, we used a nonequilibrium flow code developed at Ohio State [14,15]. The code incorporates (i) vibrational nonequilibrium of air, (ii) realistic air chemistry, including vibrationally nonequilibrium reactions, (iii) kinetics of free electrons heated by the field (vibrational and electronic excitation, ionization,

recombination, and attachment), (iv) ionization by a high-energy e-beam, and (v) one-dimensional gas dynamics. The code explicitly uses a master equation to calculate the vibrational level populations of N_2, O_2, and NO, and a coupled Boltzmann equation to calculate the free electron energy distribution function. The code has been extensively validated by comparison with numerous experiments, such as electron swarm data in N_2, O_2, and air [16,17], nonequilibrium NO formation behind the shock wave [14], and alkali-seeded and unseeded air MHD accelerator performance data [15].

To explore the issues raised in Section 1, we first used the code to model an air plasma initially at equilibrium at P=1 atm, T=2000 K ($n_e \cong 3 \cdot 10^6$ cm^{-3}). A constant electric field is applied to the plasma, thereby heating free electrons, producing more ionization, and slowing down electron-ion recombination, until complete steady state is reached. Such a process models applying a transverse DC or RF bias to a pair of electrodes in the already relatively hot plasma. The 2,000 K temperature is chosen to represent the maximum temperature allowable by the research goal. For this initial modeling, this gas temperature is assumed constant, i.e. all Joule heat is removed. Results of the calculations are summarized in Fig. 1. It can be seen that electron densities in excess of $n_e=10^{13}$ cm^{-3} can be reached at electron temperatures of T_e~17,000 K (a typical value of T_e in glow discharges, see Fig. 1(a,b)). At these conditions, the power to sustain $n_e=10^{13}$ cm^{-3} exceeds 30 GW/m^3 (see Fig. 1(c)). The prohibitively high power budget is entirely due to the extremely inefficient ionization. Indeed, from Fig. 1(d), one can see that less than 0.1% of the input power goes into direct ionization. This means that the remaining 99.9% goes to vibrational and electronic excitation (and ultimately to heat), i.e. is wasted. Although vibrational excitation of the gas somewhat improves ionization efficiency, this effect is not very significant (within a factor of two).

It is obvious that a dramatic power budget reduction can be potentially achieved by increasing ionization efficiency. For example, improving the ionization efficiency from 0.1% to 100% would reduce the power budget by about 3 orders of magnitude, down to ~30 MW/m^3. This level of power reduction can be approached by producing ionization by a high-power electron beam, instead of using an electric field, or by short duration high-voltage high repetition rate pulses.

In the second series of calculations, an equilibrium air plasma at P=1 atm, T=2000 K is excited by a uniform electron beam, until complete steady state is reached. Again, the gas temperature is assumed to remain constant at 2,000 K. Results are shown in Fig. 2. It can be seen that the power budget at $n_e=10^{13}$ cm^{-3} is dramatically reduced, down to 60 MW/m^3 (i.e. by a factor of 500 compared to field ionization). This power loading corresponds to an e-beam current density of j_{beam}=20 mA/cm^2. The ionization efficiency of the beam is 44%. Note that the use of a high-energy electron beam is equivalent to heating the electrons up to very high energies (10 keV and higher), compared to the electron heating by an electric field (1-2 eV). We emphasize that it is the use of these high electron energies that allows a dramatic increase in ionization efficiency. Figure 3 plots the power budget of the electric field sustained and e-beam sustained air plasmas as a function of the electron density. Further power budget reduction might be achieved only by reducing the electron removal rates. In particular, recent results obtained in nonequilibrium plasmas optically pumped by a CO laser [12,13] suggest that production of large amounts of metastable species in the plasma may result in a significant reduction of both dissociative recombination and the electron attachment rates.

In the next two series of calculations, the gas temperature is no longer assumed constant, and gas heating by the applied field or by the e-beam is allowed. The gas is flowing in a constant cross section area adiabatic channel 10 cm in diameter, with an initial velocity of 100 m/s, and (a) with a uniform electric field of 2500 V/cm, or (b) with a uniform e-beam with a current density of j_{beam}=20 mA/cm^2 applied in the channel. Results are summarized in Fig. 4. It can be seen that if ionization is produced by the field, at $x \cong 6$ cm both electron density and temperature sharply increase. This occurs because ionization is strongly coupled to gas heating by the field (so-called runaway ionization or heating instability [1,2]). It might be difficult to delay this runaway ionization since this would require extremely rapid heat removal. A nonequilibrium plasma with $n_e=10^{13}$ cm^{-3} is therefore not likely to be sustained over distances longer than ~1 mm (or ~1 cm if the initial flow velocity is 1000 m/s). This type of behavior represents a well-known effect of the glow-to-arc transition in a positive column of the glow discharge. This effect would result in a major collapse of the entire discharge, so that the nonequilibrium plasma

conditions could not be sustained. On the other hand, if ionization is produced by an e-beam, no runaway ionization occurs, and the gas temperature profile becomes much more uniform (see Fig. 4).

In the final series of calculations, the approach is the same as for the conditions of Fig. 4 but the channel is no longer adiabatic. Gas temperature is prevented from rising and kept nearly constant by tailoring the wall heat flux. It is assumed that the axial temperature profile is uniform (one-dimensional flow model). The results are summarized in Fig. 5. It can be seen that if ionization is produced by the field, keeping the temperature nearly constant at T=2000 K, sustaining the electron density of $n_e=10^{13}$ cm^{-3} would require a wall heat flux of nearly 80 kW/cm^2. For a 1 m diameter channel, the calculated wall flux reaches about 800 kW/cm^2. On the other hand, if ionization is produced by an e-beam, the wall heat flux to keep the gas temperature nearly constant is about 150 W/cm^2 (or 1.5 kW/cm^2 for a 1 m diameter channel).

The one-dimensional kinetic model used in the present calculations correctly predicts the onset of the heating instability development (such as constriction of the positive column of a glow discharge, see Fig. 4). However, it cannot predict the plasma conditions within the constricted discharge. First, the model does not take into account the external circuit, in particular, the ballast resistor that limits the discharge current and prevents the runaway ionization. Also, the model does not incorporate transport processes such as electron diffusion and heat conduction that may delay the heating instability development to some extent, and which control the diameter and the temperature of the constricted discharge. To illustrate the role of these processes in sustaining thermodynamic nonequilibrium and control of stability in high-pressure air discharges, the next section discusses the experiments and the modeling of the high-voltage atmospheric pressure discharge in air.

3. Studies of a high-voltage atmospheric pressure discharge in air

3.1. Experimental

This type of electric discharge has been developed in the 1980's at Chemical Physics Laboratory of A.V.Lykov Heat and Mass Transfer Institute in Minsk, USSR [5-9]. The primary applications of the discharge have been in nonequilibrium plasma chemical synthesis, such as energy-efficient oxidation of atmospheric nitrogen [5] and dissociation of carbon dioxide [6], and in plasma material processing, such as nitriding of metal surfaces [7] and saturation of the high-temperature superconductors with oxygen [8]. This axial DC discharge is sustained between two pin or ring electrodes, typically 2 to 10 cm apart, in a quartz tube of 3-20 mm internal diameter. For large electrode separations, a separate pre-ionization circuit is used to first initiate the discharge between the cathode and the pre-ionization anode (see Fig. 6). In some cases, movable cathode has been used instead. The test gases enter the discharge tube from the cathode side and are exhausted into the atmosphere. The outer surface of the discharge tube can be cooled either by natural convection of air or by water. The discharge is powered by a 3 kW DC power supply providing a maximum current of 200 mA. The discharge voltage and current can be varied in a range U=2-12 kV and I=30-200 mA, respectively. The mass flow rate through the discharge can be varied in a range G=100-800 g/hour. The discharge can be sustained in air, nitrogen, oxygen, and carbon dioxide at atmospheric pressure. In experiments with air, room air has been used and NO concentration has been measured in the discharge exhaust using analytical chemistry methods. The gas temperature at the discharge tube exit (a few cm downstream of the anode) has been measured using a Pt – Pt/Rh thermocouple.

3.2 Kinetic Model

Kinetic models and computer codes for modeling of high-voltage atmospheric pressure discharges in nitrogen, oxygen, and air have also been previously developed at Chemical Physics Laboratory [9,18-20], and further modified at Ohio State. In the present paper, we use a two-dimensional nonequilibrium flow code [9] coupled with the key relaxation and chemical processes occurring in the air plasma [18]. The model incorporates the following kinetic processes:

$$N_2 + e^- \rightarrow N_2(v) + e^-, \quad v = 1-8 \tag{1}$$

$$O_2 + e^- \rightarrow O_2(v) + e^-, \quad v = 1-3 \tag{2}$$

$$\begin{gathered} AB(v) + M \rightarrow AB(v-1) + M, \\ AB = N_2, O_2, NO; \qquad M = N_2, O_2, N, O, NO \end{gathered} \tag{3}$$

$$AB(v) + CD(w-1) \rightarrow AB(v-1) + CD(w); \quad AB, CD = N_2, O_2, NO \tag{4}$$

$$O_2 + e^- \rightarrow O + O \tag{5}$$

$$N_2(v) + M \Leftrightarrow N + N + M \tag{6}$$

$$O_2(v) + M \Leftrightarrow O + O + M \tag{7}$$

$$NO(v) + M \Leftrightarrow N + O + M \tag{8}$$

$$N_2(v) + O \Leftrightarrow NO + N \tag{9}$$

$$O_2(v) + N \Leftrightarrow NO(w) + O \tag{10}$$

In Eqs. (1-10), v and w are the vibrational quantum numbers. This list of kinetic processes is based on the sensitivity analysis conducted using a much more detailed state-specific kinetic model discussed in Section 1 for modeling of relatively high-temperature (T>1500 K) nonequilibrium ionized reacting air flows [15]. The selected processes appear to be, by far, the most critical in such flows. At these temperatures, the vibrational mode disequilibrium of nitrogen and oxygen is not expected to be very strong. Therefore, vibrational kinetics of diatomic species is considered in the harmonic oscillator approximation.

The rates of vibrational excitation of N_2 and O_2, as well as of oxygen dissociation by electron impact are obtained from the solution of the Boltzmann equation [21]. The vibration-translation (V-T) relaxation times, as well as the rates of the vibration-vibration (V-V) energy exchange among the different diatomic species are taken to be the same as in [18]. The rates of the thermal chemical reactions are taken from [22]. The model assumes a simple dependence of the vibrationally stimulated state-specific chemical reaction rates k(v,T) on the vibrational quantum number [18],

$$k(v,T) \sim \begin{cases} A(T)\exp\left(-\dfrac{E_A - \theta v}{T}\right), & v \le \dfrac{E_A}{\theta} \\ A(T), & v > \dfrac{E_A}{\theta} \end{cases} \tag{11}$$

where A(T) and E_A are the pre-exponential factor and the activation energy in the Arrhenius expression for the thermal reaction rate coefficient k(T), respectively, and θ is the characteristic vibrational energy of a diatomic molecule. The state-specific rates k(v,T) are normalized on the thermal reaction rate coefficient.

The rate of electron impact ionization is determined from the following relation [23],

$$k_{ion} = A \cdot \exp\left[-\frac{B}{E/N} + \frac{Cz}{(E/N)^2} \right], \quad z = \exp\left[-\theta(N_2)\left(\frac{1}{T_v(N_2)} - \frac{1}{T} \right) \right] \qquad (12)$$

where A is the electron-neutral collision frequency, E/N is the reduced electric field, $\theta_1(N_2)$=3353 K and $T_v(N_2)$ are characteristic vibrational energy of nitrogen and vibrational temperature of N_2, respectively. The coefficient B in Eq. (12) is a parameter adjusted to make the calculated discharge voltage equal to the experimentally measured voltage. This allows implicitly incorporating multiple electron impact ionization processes occurring in the discharge, including stepwise ionization from the electronically excited levels, whose rates have the same type exponential dependence on E/N. On the other hand, this approach also allows the overall power added to the discharge to be consistent with the experimental value. The last term in the exponential factor in Eq. (9) takes into account the effect of the superelastic collisions between electrons and nitrogen molecules on the impact ionization rate. The value of a coefficient C=43.5, obtained from the solution of the Boltzmann equation for the plasma electrons in air [23], turns out to be nearly the same for all high energy threshold impact excitation processes including such as excitation of electronic levels and ionization. The electron-ion recombination coefficient is taken as $\beta_{ei}=2\cdot10^{-7}(T/T_e)^{-0.5}$ cm^3/sec [1]. At the relatively high temperatures of T>1500 K, the effect of the complex ions such as N_4^+ and O_4^+, as well as the negative ions such as O_2^- and O^- is expected to be insignificant.

The model incorporates the parabolized Navier-Stokes equations in cylindrical geometry, the equations for the vibrational mode energies of N_2, O_2, and NO, the electron density equation, and the species concentration equations for N, N_2, O, O_2, and NO (see Appendix). The plasma is assumed to be quasineutral. The pressure gradient and the electric field at each axial location are found from the mass flow rate conservation and the discharge current conservation, respectively. Both the pressure gradient and the electric field are assumed to be changing only the axial direction. For these reasons, the model is not applicable for simulation of the flow field and the plasma kinetics near the discharge electrodes.

The boundary condition for the gas temperature on the wall is determined from the equality of the heat flux from the plasma into the wall and the discharge tube external cooling rate due to both natural convection by air and radiation (see Appendix).

3.3. Results and Discussion

Figure 7 shows a photograph of the discharge running in air at U=2.0 kV, I=50 mA, and G=240 g/hour. The discharge is sustained between a movable pin cathode and an annular anode 3 cm apart. The discharge tube internal diameter is 2 cm, while the apparent plasma diameter is much smaller, only about 4-8 mm. This implies that the discharge is in fact not wall-stabilized, unlike low-pressure diffuse glow discharges. In other words, the positive column of the discharge is already constricted, as discussed in Section 2.

Voltage current characteristics of the discharge in air for the tube diameter of 3.2 mm and the electrode separation of 5 cm and 7.5 cm are shown in Fig. 8. One can see that the discharge has a falling voltage current characteristic, which indicates that it is sustained in the abnormal glow-to-arc transition regime [1,2] (region FG in Fig. 9), i.e. it is inherently unstable. The discharge stability in this case is controlled by a ballast resistor connected in series with the discharge tube, which limits the total current and prevents the discharge from converting into a high current arc. The limiting current, shown in Fig. 9, is $I_{max}=E_{max}/R$, where E_{max} is the maximum e.m.f. of the power supply, and R is the ballast resistance [1]. The voltage current characteristic of the discharge and the ballast resistor together is rising. From the data of Fig. 9, the power density in the discharge is in the range 0.5-1.0 kW/cm^3. The fraction of the total power delivered by the power supply dissipated by the ballast resistor is 40-60%.

Figure 10 plots the calculated cross-section averaged gas temperature and the experimental temperature at the exit of the 12.5 long discharge tube for the electrode separation of 5 cm (i.e. 7.5 cm downstream of the anode), showing good agreement. Figure 11 compares the experimental and the calculated mole fractions of nitric oxide at the exit of the discharge. The agreement is fair although one

can see that the model underpredicts the NO concentrations by about a factor of two. We believe this to be mainly due to the use of a simplified kinetic model described in Section 3.2. However, the results displayed in Figs. 10,11 show that the model satisfactorily describes the kinetics and the overall energy balance of the discharge.

Figures 12-15 display various discharge plasma parameters for the following conditions: U=7.6 kV, I=40 mA, G=700 g/hour. Figure 12 plots the gas temperature, the vibrational temperature of N_2, and the electron temperature on the centerline of the discharge tube. Figure 13 shows the mole fractions of oxygen atoms and NO molecules, as well as the ionization fraction at the centerline. Figure 14 plots the radial distributions of the temperatures at the discharge exit (x=5 cm). Finally, Fig. 15 shows the axial distribution of the electron density at x=0.5, 1.3, and 3.0 cm. From these results, it is clear the ionization heating instability develops at $1.0<x<1.5$ cm, with both the electron density and the gas temperature on the centerline rapidly rising, so that the discharge becomes constricted at x=1.3 cm (see Figs. 12,13). However, no runaway ionization (see Fig. 3) predicted by the one-dimensional model discussed in Section 2 occurs in this case. In the constricted discharge, the conditions at the centerline, where the electron density reaches $n_e \cong 10^{13}$ cm^{-3}, remain far from thermodynamic equilibrium (see Fig. 14,15). This occurs because the ballast resistor limits the total discharge current preventing it from short-circuiting and converting it into a hot equilibrium arc. In addition, the ambipolar diffusion prevents the high-current zone from shrinking below a few millimeters diameter, thereby limiting the current density and the centerline temperature. This effect makes the constricted discharge more diffuse at x>1.3 cm, reducing the electron density on the centerline (see Figs. 13,15).

Figure 16 presents the ratio of the discharge power going into ionization to the total discharge power. One can see that the ionization efficiency of the discharge is of the order of 0.1%. This result is generally consistent with the predictions of the detailed state-specific kinetic model discussed in Section 2 (see Fig. 1(c)).

4. Summary

The calculations of the atmospheric pressure air plasma power budget (Section 2) suggest that, if ionization is produced by an electric field, an electron density of $n_e=10^{13}$ cm^{-3} is sustained at a power budget of more than 30 GW/m^3. This is due to the extremely low ionization efficiency (less than 0.1%) that prevails in nonequilibrium electric discharges (DC, AC, and RF). Therefore, the sole use of large-volume self-sustained discharges, whether the electric field is DC, RF, or microwave, is not feasible from the energy efficiency point of view.

A substantial part of the needed power budget reduction can be achieved by using an efficient external ionization source, such as an e-beam (ionization efficiency up to 40-50%). This will require 60 MW/m^3 to sustain electron density of $n_e=10^{13}$ cm^{-3}, if the electron removal process is not modified. A similar result can be potentially achieved by using short duration, high-voltage, high repetition rate pulses [3]. At the reduced electric field of $E/N=3\cdot10^{-15}$ $V\cdot cm^2$, which in 2000 K air corresponds to the electric field of E~10 kV/cm, ionization efficiency of such pulses can reach approximately 10% [1]. Further power budget reduction from the 60 MW/m^3 level achieved by efficient ionization can be produced only by reducing the rate of electron removal. This may well be achieved by producing large amounts of metastable (e.g. vibrationally excited) species in the CO-seeded air using an efficient laser [12,13].

Calculations using a quasi-one-dimensional kinetic model (Section 2) suggest that the required electron density is reached under conditions where plasma collapse may be likely and glow-to-arc transition may be difficult to control over long distances. This occurs due to strong coupling between ionization and heating. However, analysis of the experiments in the high-voltage atmospheric pressure discharge in air (Section 3), as well as calculations using a two-dimensional model of the discharge, show that the use of ballast resistor stabilization allows sustaining a stable constricted nonequilibrium atmospheric pressure air discharge well into the arc transition regime. The region occupied by the constricted discharge is a few cm long and a few mm in diameter. The diameter of the plasma is primarily controlled by the ambipolar diffusion of the charged species out of the high-current region. The plasma volume can be scaled up by using multiple separately ballasted cathodes [24]. The results of calculations

show that the two-dimensional kinetic model used gives an adequate description of the kinetics and the energy balance of the high-voltage atmospheric pressure discharge in air. The calculations of the discharge ionization efficiency are consistent with the predictions of the detailed state-specific kinetic model discussed in Section 2.

5. Acknowledgements

This research was supported by the Director of Defense Research and Engineering (DDR&E) within the Air Plasma Pamparts MURI Program managed by AFOSR. We would also like to express our gratitude to Dr. Sergey Macheret for numerous fruitful discussions and useful suggestions.

6. Appendix. Governing equations for the two-dimensional model of the air discharge

Motion equations for cylindrical geometry:

$$\frac{\partial(\rho u)}{\partial x}+\frac{1}{r}\frac{\partial(\rho v r)}{\partial r}=0 \tag{13}$$

$$\rho u\frac{\partial u}{\partial x}+\rho v\frac{\partial u}{\partial r}=\frac{1}{r}\frac{\partial}{\partial r}\left(r\eta\frac{\partial u}{\partial r}\right)-\frac{dP}{dx} \tag{14}$$

Kinetic mode energy equation:

$$\begin{aligned}\rho c_P u\frac{\partial T}{\partial x}+\rho c_P v\frac{\partial T}{\partial r}=\frac{1}{r}\frac{\partial}{\partial r}\left(r\lambda\frac{\partial T}{\partial r}\right)+jE(1-\sum_i\alpha_{vib,i})+\rho R_0\sum_i\frac{x_i}{\mu_i}\frac{\varepsilon_{vib,i}-\varepsilon_{vib,i}(T)}{\tau_{VT,i}}\\ -\rho\sum_i\left[h_i-\frac{R_0}{\mu_i}\varepsilon_{vib,i}(T)\right]\left(\frac{dx_i}{dt}\right)_{chem}-\rho\sum_i\frac{R_0}{\mu_i}x_i\left(\frac{d\varepsilon_i}{dt}\right)_{chem}\end{aligned} \tag{15}$$

Vibrational mode energy equations (N_2, O_2, NO):

$$\begin{aligned}\rho x_i u\frac{\partial\varepsilon_{vib,i}}{\partial x}+\rho x_i v\frac{\partial\varepsilon_{vib,i}}{\partial r}=\frac{1}{r}\frac{\partial}{\partial r}\left(r\rho x_i D\frac{\partial\varepsilon_{vib,i}}{\partial r}\right)+\frac{jE\alpha_{vib,i}}{R_0/\mu_i}-\rho x_i\frac{\varepsilon_{vib,i}-\varepsilon_{vib,i}(T)}{\tau_{VT,i}}\\ +\rho\sum_i x_i\left(\frac{d\varepsilon_i}{dt}\right)_{chem}\end{aligned} \tag{16}$$

Electron density equation:

$$\frac{\rho}{\mu}u\frac{\partial y_e}{\partial x}+\frac{\rho}{\mu}v\frac{\partial y_e}{\partial r}=\frac{1}{r}\frac{\partial}{\partial r}\left(r\frac{\rho}{\mu}D_a\frac{\partial y_e}{\partial r}\right)+\left(\frac{\rho}{\mu}\right)^2\left(k_{ion}y_e-\beta y_e^2\right);\quad y_e=\frac{n_e}{N} \tag{17}$$

Species concentration equations (N, N_2, O, O_2, NO):

$$\rho u\frac{\partial x_i}{\partial x}+\rho v\frac{\partial x_i}{\partial r}=\frac{1}{r}\frac{\partial}{\partial r}\left(r\rho D\frac{\partial x_i}{\partial r}\right)+\rho\left(\frac{dx_i}{dt}\right)_{chem}\quad;\quad x_i=\frac{\rho_i}{\rho} \tag{18}$$

Chemical reactions considered:

$$\sum_l a_l A_l \Leftrightarrow \sum_m b_m B_m \tag{19}$$

Rate of species ***i*** concentration change due to chemical reactions (running index ***j***):

$$\left(\frac{dx_i}{dt}\right)_{chem}=\frac{\rho}{\mu}\sum_j\left[k_{f,j}\prod_l\left(\frac{x_l}{\mu_l}\right)^{a_l}-k_{r,j}\prod_m\left(\frac{x_m}{\mu_m}\right)^{b_m}\right] \tag{20}$$

Rate of species ***i*** vibrational energy change due to chemical reactions (running index ***j***):

$$\left(\frac{d\varepsilon_i}{dt}\right)_{chem}=\frac{\rho}{\mu}\sum_j\left[\varepsilon_{f,j}\prod_l\left(\frac{x_l}{\mu_l}\right)^{a_l}-\varepsilon_{r,j}\prod_m\left(\frac{x_m}{\mu_m}\right)^{b_m}\right] \tag{21}$$

Mass flow rate integral and discharge current integral (used for dP(x)/dx and E(x) calculation):

$$G=\int_0^R\rho urdr\;;\quad I=\int_0^R en_e w_{dr}(E/N)rdr \tag{22}$$

Boundary conditions on the discharge tube wall:

$$u=v=0\;;\quad \lambda\left(\frac{\partial T}{\partial r}\right)_w=(\alpha_{conv}+\alpha_{rad})(T_{wo}-T_\infty)\;;\quad T_{v,i}=T \tag{23}$$

$$(x_i)_w=0\ (atomic\ species)\;;\quad \left(\frac{\partial x_i}{\partial r}\right)_w=0\ (molecular\ species)\;;\quad (y_e)_w=0 \tag{24}$$

Species vibrational temperatures and equilibrium vibrational energies:

$$T_{v,i}=\frac{\theta_i}{\ln(1+\theta_i/\varepsilon_{vib,i})};\quad \varepsilon_{vib,i}(T)=\frac{\theta_i}{\exp(\theta_i/T)-1} \tag{25}$$

7. References

1. Raizer, Y.P., "Gas Discharge Physics", Springer-Verlag, Berlin, 1991
2. E.P. Velikhov, A.S. Kovalev, and A.T. Rakhimov, “Physical Phenomena in Gas Discharge Plasmas”, Moscow, Nauka, 1987
3. Generalov, N.A., V.P. Zimakov, V.D. Kosynkin, Yu.P. Raizer, and D.I. Roitenburg, Technical Physics Letters, vol. 1, p. 431, 1975
4. W. Rich, R.C. Bergman, and J.A. Lordi, AIAA J., vol. 13, p. 95, 1975
5. Zhdanok, S.A., Konysheva, N.B., Sergeeva, L.A., Soloukhin, R.I., and Yaremenko, A.I., "Experimental Study of Nonequilibrium Reaction of Nitrogen Oxidation in the High Voltage Atmospheric Pressure Discharge", Soviet Journal Doklady AN BSSR, Vol. 31, No. 2, p. 124-126, 1987
6. Zhdanok, S.A., Vasilieva, E.M., and Sergeeva, L.A., "Optimization of Parameters of the Nonequilibrium CO_2 Dissociation Process", Soviet Journal Vesti AN BSSR, Series Phys. Energ. Sc., No. 3, pp. 79-82, 1988
7. Zhdanok, S.A., Vasilieva, E.M., and Sergeeva, L.A., "Study of the High Voltage Atmospheric Pressure Discharge and its Application for Surface Treatment", Soviet J. of Engineering Physics, Vol. 58, No.1, pp.101-104, 1990
8. Zhdanok, S.A., Borodin, V.I., and Bumai, Yu .A., "The use of Oxygen Plasma of the High Voltage Atmospheric Pressure Discharge for Processing of High-Temperature Superconducting Ceramics", in “Heat and Mass Transfer with Phase and Chemical Transmissions”, Heat and Mass Transfer Institute of Academy of Sciences of BSSR, pp. 3-11, Minsk, 1990
9. I.V. Adamovich, P.A. Apanasevich, V.I. Borodin, S.A. Zhdanok et al., "CARS Diagnostics of High-Voltage Atmospheric Pressure Discharge in Nitrogen", Springer Proceedings in Physics, vol. 63, "Coherent Raman Spectroscopy", Eds. G. Marowsky and V.V. Smirnov, Springer, Berlin, 1992, pp. 215-223
10. Basov, N.G., Babaev, I.K., Danilychev, V.A., et al., Sov. Journal of Quantum Electronics, vol. 6, 1979, p. 772
11. A.S. Kovalev, E.A. Muratov, A.A. Ozerenko, A.T. Rakhimov, and N.V. Suetin, Sov. J. Plasma Physics, Vol. 11, 1985, p. 515
12. Ploenjes, E., Palm, P., Adamovich, I.V., and Rich, J.W., “Control of Stability and Electron Removal Rate in Optically Pumped RF Discharges” Paper 99-3665, presented at AIAA 30th Plasmadynamics and Lasers Conference, Norfolk, VA, June 28 – July 1, 1999
13. E. Plönjes, P. Palm, I.V. Adamovich, and J. W. Rich, “Ionization Measurements in Optically Pumped Discharges”, accepted for publication in Journal of Physics D: Applied Physics, 2000
14. C.E. Treanor, I.V. Adamovich, M.J. Williams, and J.W. Rich, "Kinetics of NO Formation Behind Strong Shock Waves", Journal of Thermophysics and Heat Transfer, vol. 10, No. 2, 1996, pp. 193
15. I.V. Adamovich, J.W. Rich, and G.L. Nelson, “Feasibility Study of Magneto-hydrodynamics Acceleration of Unseeded and Seeded Air Flows”, AIAA Journal, vol. 36, No. 4, 1998, pp. 590-597
16. L.G.H. Huxley and R.W. Crompton, “The Diffusion and Drift of Electrons in Gases”, Wiley, New York, 1974
17. J.W. Gallagher, E.C. Beaty, J. Dutton, and L.C. Pitchford, J. Phys. Chem. Ref. Data, vol.12, 1983, p. 109
18. Zhdanok, S.A., Borodin, V.I., and Chernukho, A.P.," Numerical Modeling of the Nitrogen Oxidation Process in the High Voltage Atmospheric Pressure Discharge", Proceedings of International School-Seminar "Modern Problems of Heat and Mass Transfer in Chemical Technology", Heat and Mass Transfer Inst. AN BSSR, pp.87-89, Minsk,1987
19. I.V. Adamovich, V.I. Borodin, S.A. Zhdanok, and A.P. Chernukho, “Numerical Modeling of Oxygen Plasma of the High Voltage Atmospheric Pressure Discharge. One-Dimensional Approach”, in “Heat and Mass Transfer at Phase and Chemical Transformations”, ITMO Press, Minsk, USSR, 1990, pp. 86-90

20. P.I. Porshnev, “Energy Balance in the Positive Column of the Axial Gas Discharge at Atmospheric Pressure”, Soviet Engineering Physics Journal, Vol. 58, No. 5, 1990, p. 814
21. N.L. Aleksandrov, F.I. Vysikailo, R.Sh. Islamov, I.V. Kochetov, A.P. Napartovich, and V.G. Pevgov, “Electron Distribution Function in a N_2:O_2=4:1 Mixture”, High Temperature, Vol. 19, 1981, p. 22
22. O.E. Krivonosova, S.A. Losev, V.P. Nalivaiko, Yu.K. Mukoseev, and O.P. Shatalov, “Recommended Data on the Rates of Chemical Reactions between Molecules Consisting of N and O atoms”, in “Khimiya Plasmy” (Plasma Chemistry), ed. by B.M. Smirnov, vol. 14, 1987, pp. 3-31
23. N.L. Aleksandrov, A.M. Konchakov, and E.E. Son, Sov. J. Plasma Phys., Vol. 4, 1978, p. 169
24. Yu.S. Akishev, A.A. Deryugin, V.B. Karal'nik, I.V. Kochetov, A.P. Napartovich, and N.I. Trushkin, Plasma Physics Reports, Vol. 20, 1994, p. 511

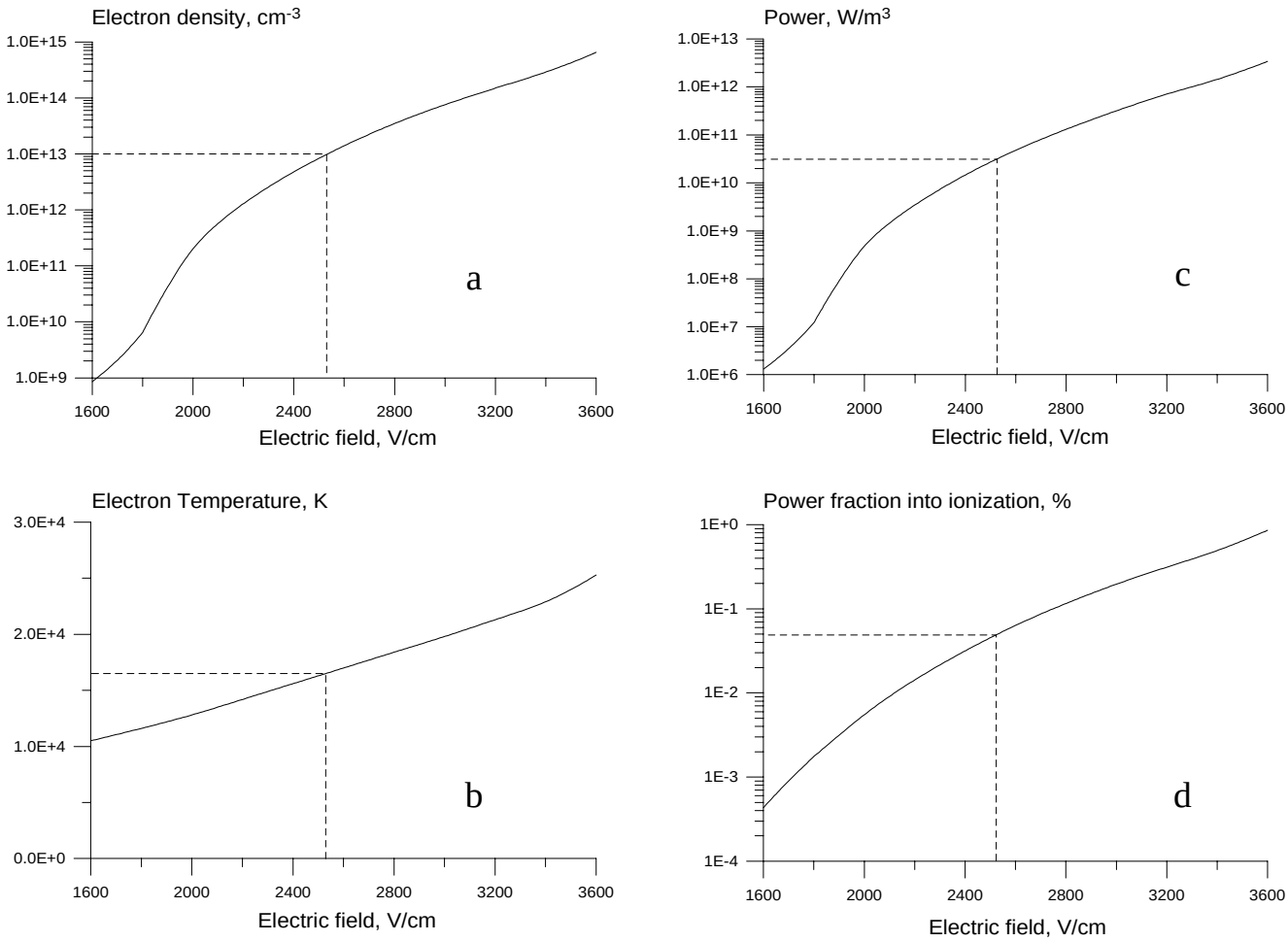

Figure 1. Summary of the steady-state plasma parameters as functions of electric field.

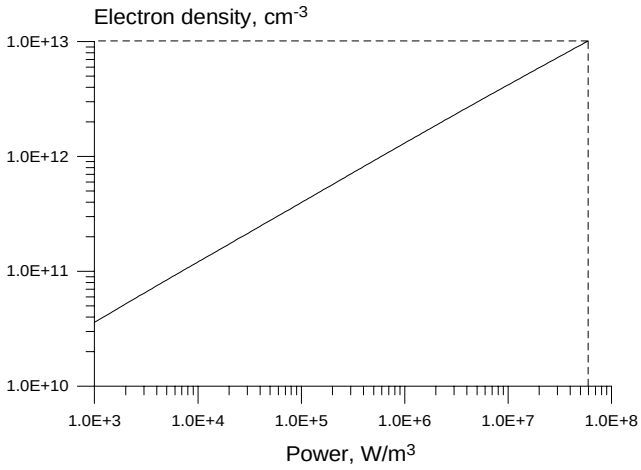

Figure 2. Electron concentration in air as a function of electron beam power absorbed. The power loading of 58 mW/m^3 corresponds to the beam current density of j_{beam}=20 mA/cm^2

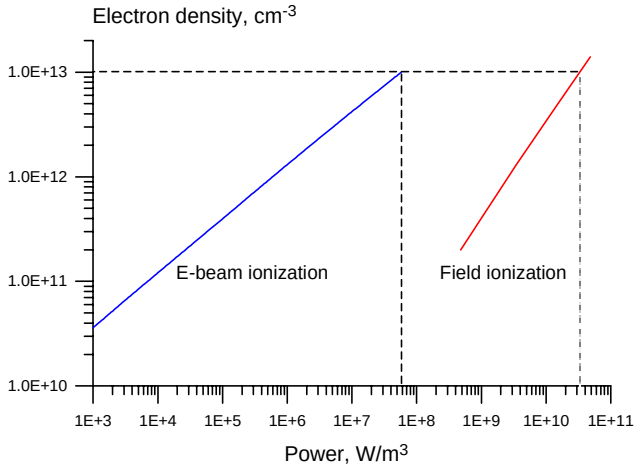

Figure 3. Comparison on the power budget of the electric field sustained and e-beam sustained air plasmas

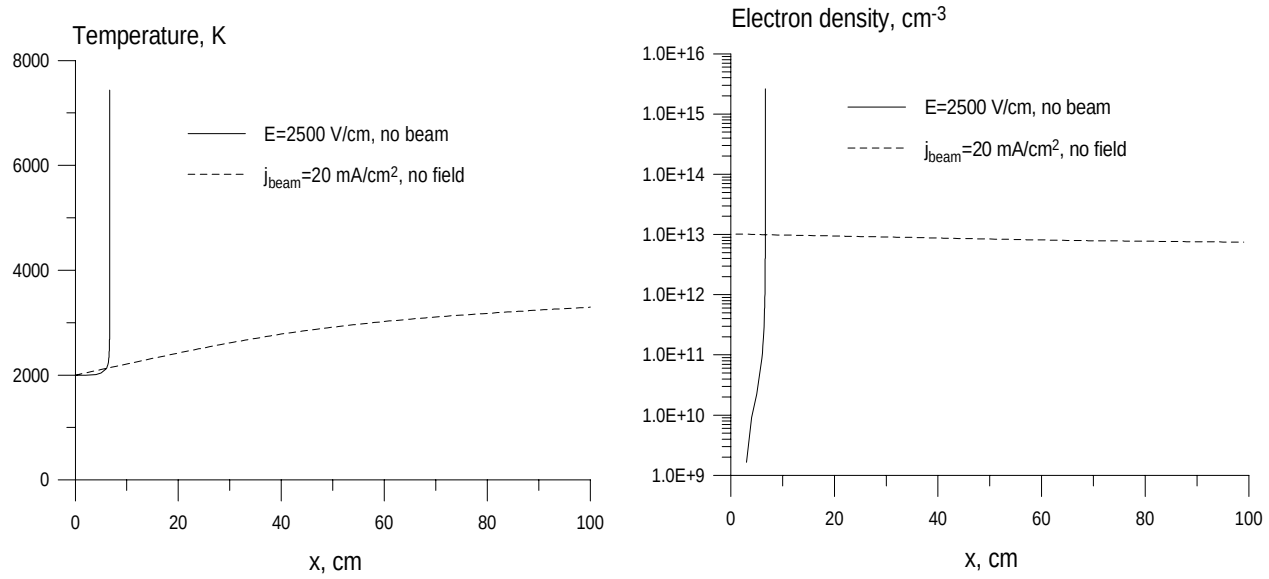

Figure 4. Heating and ionization in air plasma flow in an adiabatic channel 10 cm in diameter. Initial conditions: air at P=1 atm, T=2000 K, u=100 m/s

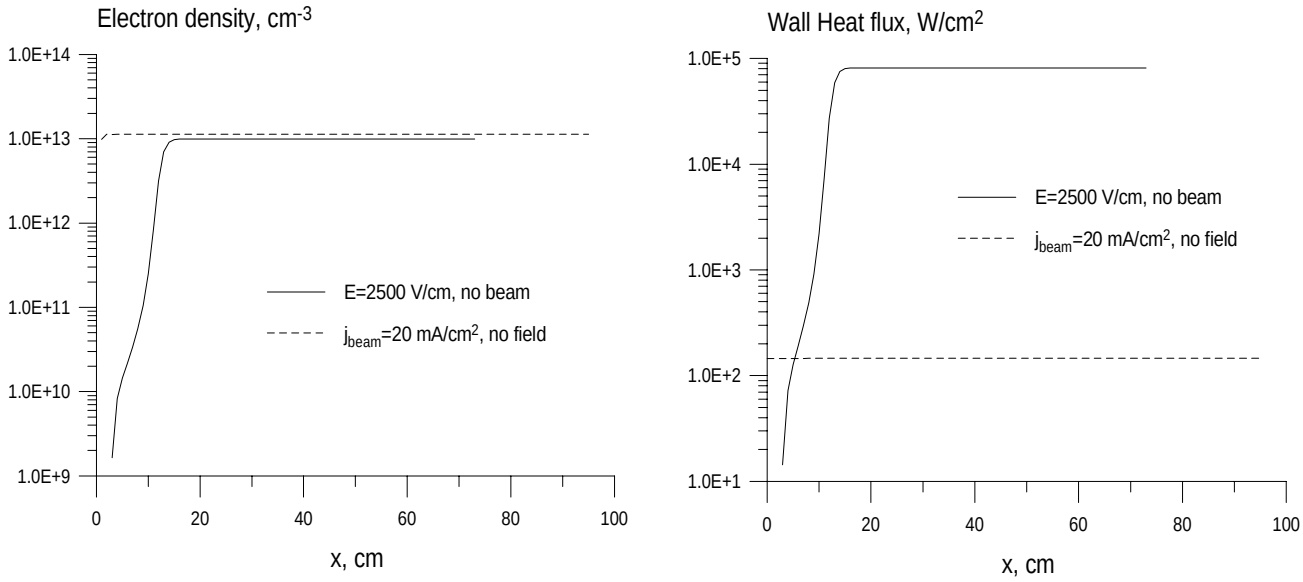

Figure 5. Ionization and wall heat fluxes in air plasma flow in a constant temperature channel 10 cm in diameter. Initial conditions: air at P=1 atm, T=2000 K, u=100 m/s

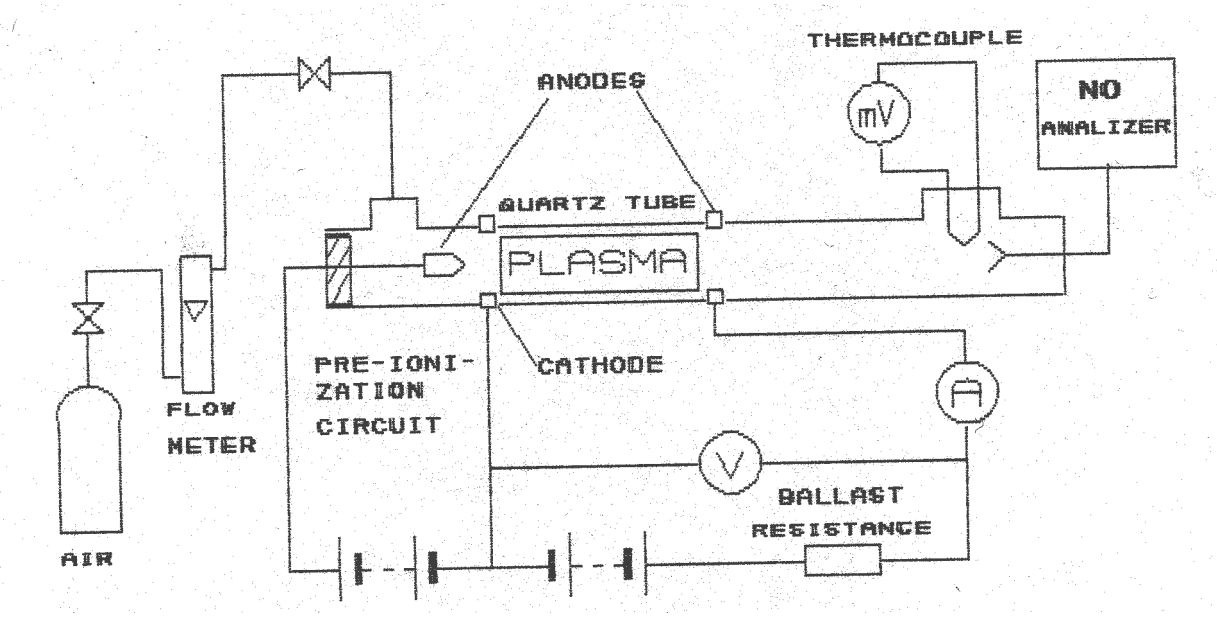

Figure 6. Schematic of the experimental setup

Figure 7. Photograph of a typical high-voltage atmospheric pressure discharge in air. U=2.0 kV, I=50 mA, G=240 g/hour, discharge tube diameter is 2 cm, distance between the electrodes is 3 cm.

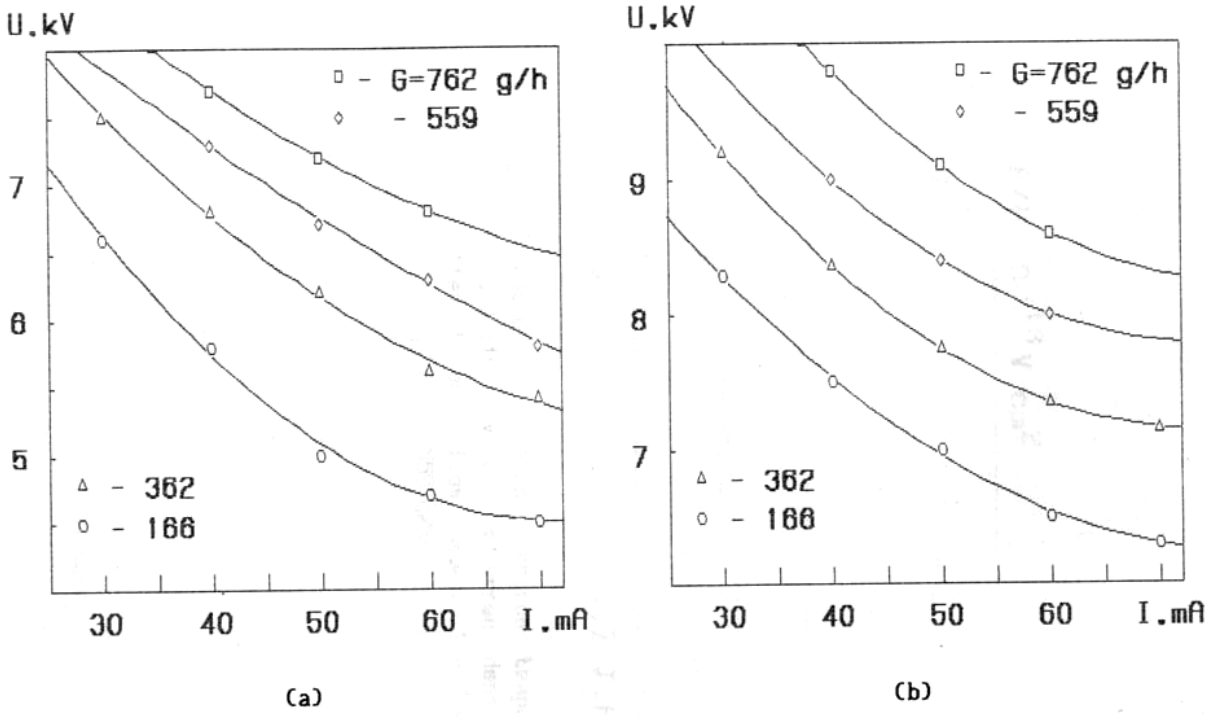

Figure 8. Voltage current characteristics of the air discharge in a 3.2 mm diameter tube at different mass flow rates for two distances between the electrodes. (a) L=5.0 cm; (b) L=7.5 cm

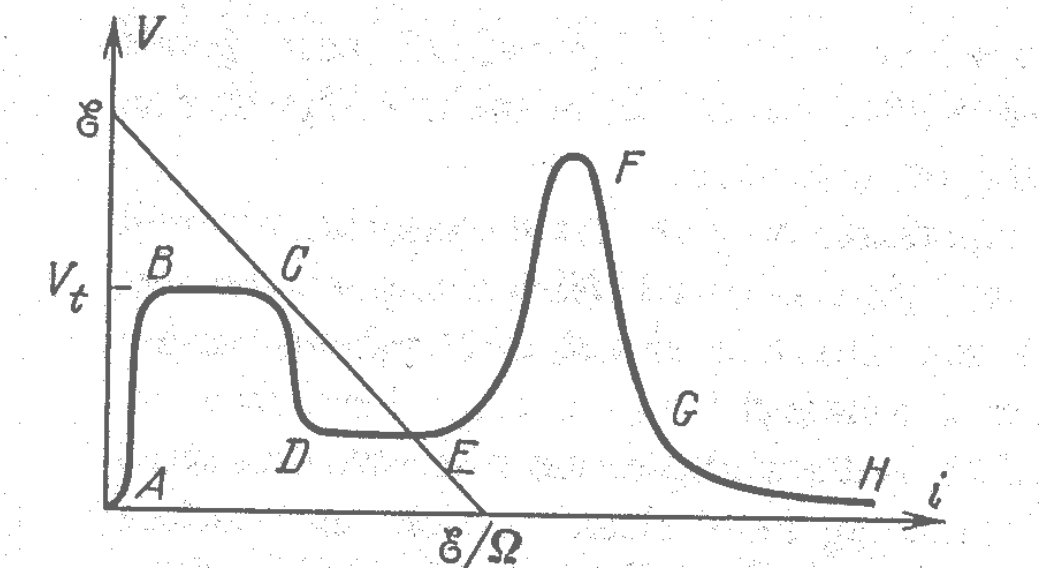

Figure 9. Qualitative voltage current characteristic of a DC discharge in a wide range of currents shown together with the loading line [1]. A, non-self-sustained Thomson discharge; BC, Townsend dark discharge; CD, transition to glow discharge DE, normal glow discharge; EF, abnormal glow discharge; FG, transition into an arc regime; GH, arc

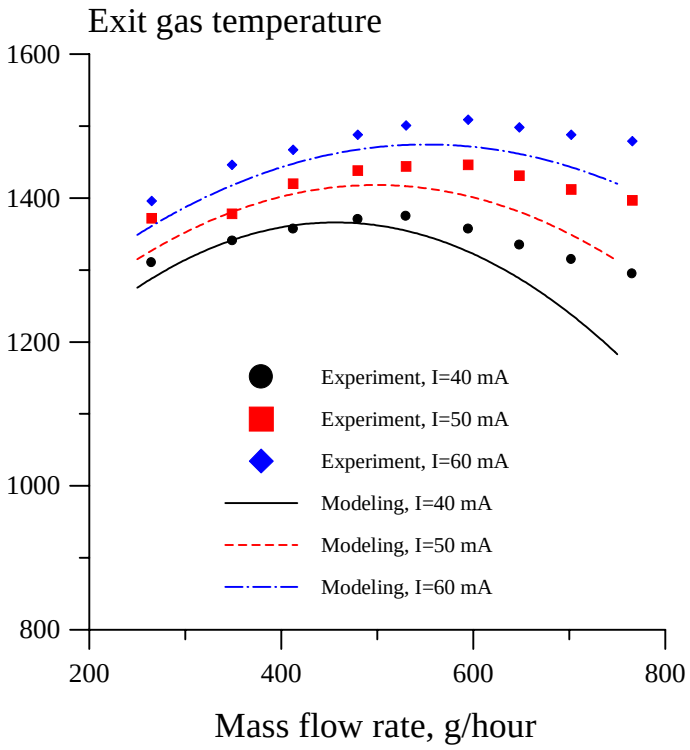

Figure 10. Comparison of the experimental and calculated gas temperatures at the exit of the discharge tube. Electrode separation is 5 cm, discharge tube length is 12.5 cm

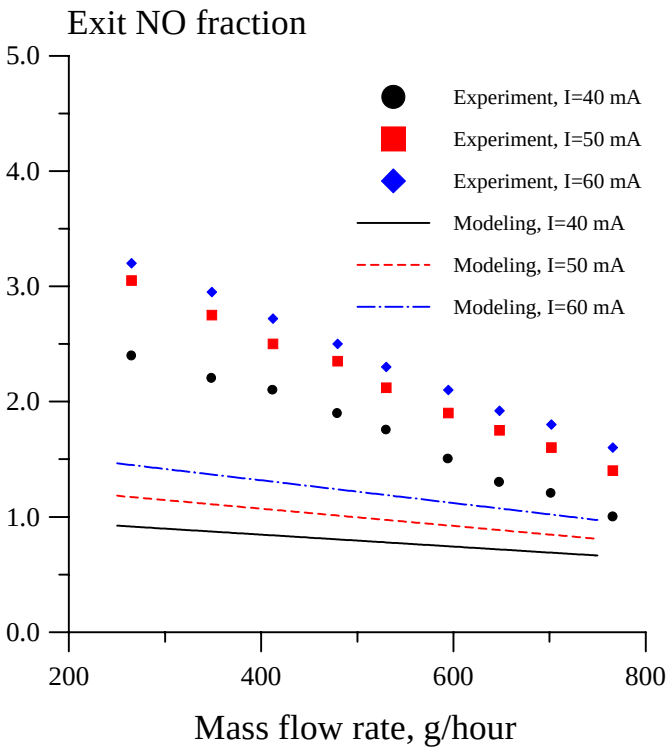

Figure 11. Comparison of the experimental and calculated NO mole fractions at the exit of the discharge tube. Electrode separation is 5 cm, discharge tube length is 12.5 cm

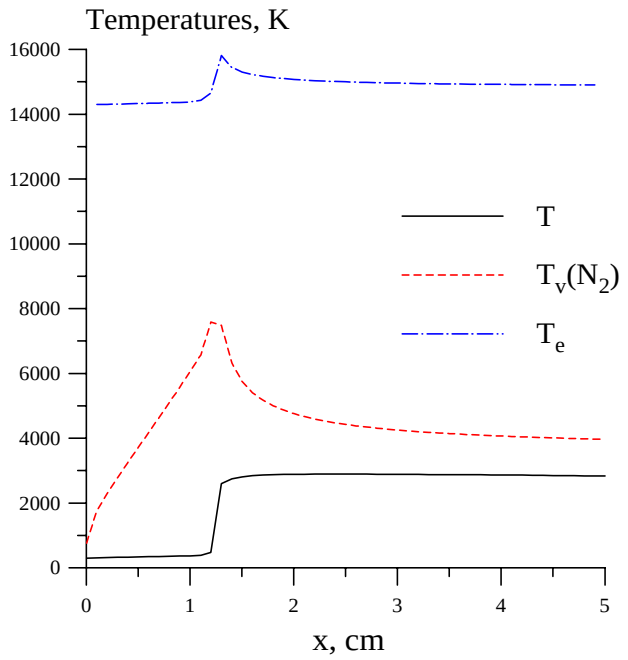

Figure 12. Axial distributions of gas temperature, vibrational temperature of N_2, and electron temperature on the discharge centerline

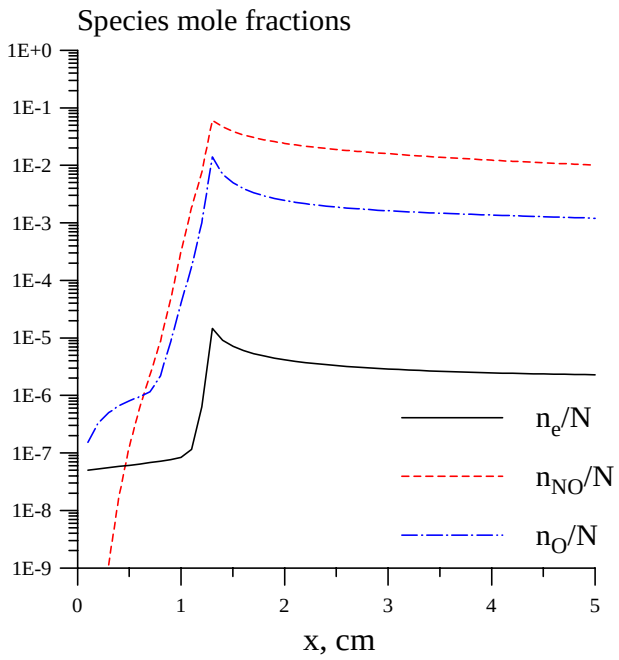

Figure 13. Axial distributions of ionization fraction, NO mole fraction, and O atom mole fraction on the discharge centerline

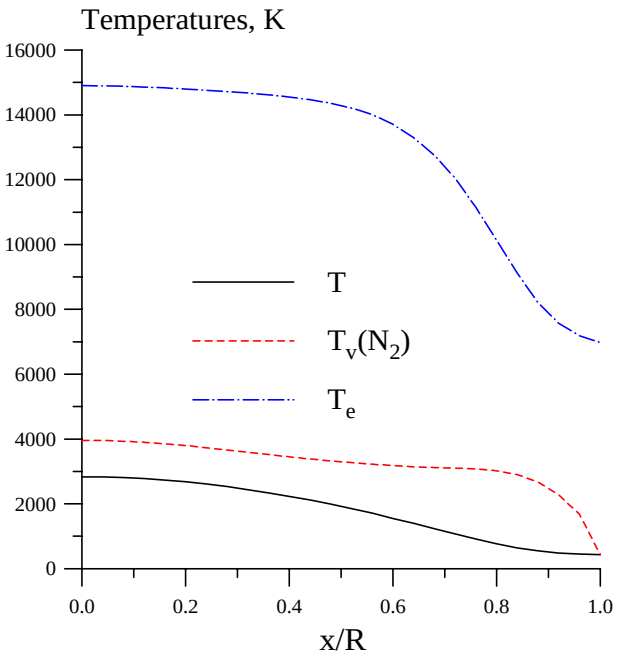

Figure 14. Radial distributions of gas temperature, vibrational temperature of N_2, and electron temperature at the discharge exit (x=5 cm)

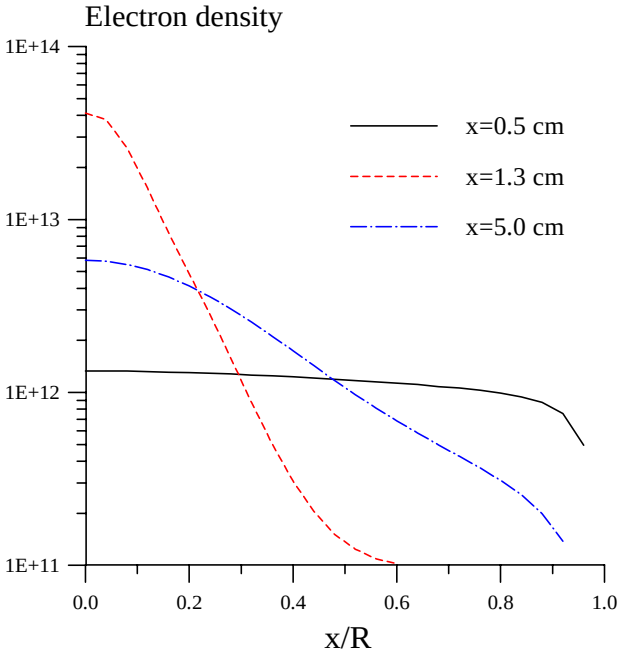

Figure 15. Radial distributions of electron density at different axial locations

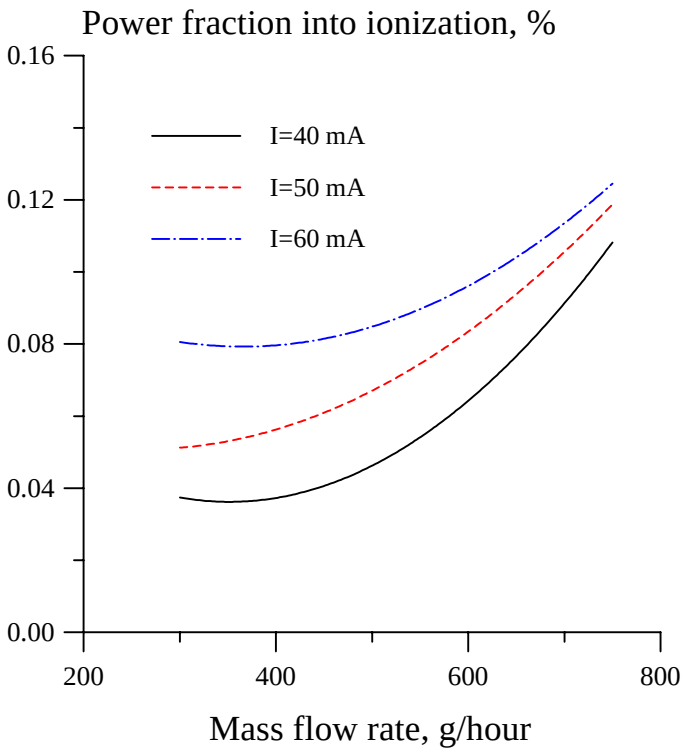

Figure 16. Calculated discharge power fraction going into ionization by electron impact for the conditions of Figs. 10,11